energies

MDPI

Article

Power Generation Analysis of Terrestrial Ultraviolet-Assisted Solid Oxide Electrolyzer Cell

Muhammad Salim Butt [1], Hifsa Shahid [1,*], Farhan Ahmed Butt [1], Iqra Farhat [1], Munazza Sadaf [2], Muhammad Raashid [3] and Ahmad Taha [4]

[1] Department of Electrical Engineering, New Campus, University of Engineering and Technology Lahore, Lahore 39021, Pakistan; salimbutt@uet.edu.pk (M.S.B.); farhanbutt@uet.edu.pk (F.A.B.); Iqra.farhat@uet.edu.pk (I.F.)
[2] Department of Electrical Engineering, FSD Campus, University of Engineering and Technology Lahore, Lahore 38070, Pakistan; munazzasadaf@uet.edu.pk
[3] Department of Chemical, Polymer and Composite Materials Engineering, New Campus, University of Engineering and Technology, Lahore 39021, Pakistan; engr_raashid@uet.edu.pk
[4] James Watt School of Engineering, University of Glasgow, Glasgow G12 8QQ, UK; ahmad.taha@glasgow.ac.uk
* Correspondence: h.shahid@uet.edu.pk

Abstract: This paper presents a novel system design that considerably improves the entrapment of terrestrial ultraviolet (UV) irradiance in a customized honeycomb structure to produce hydrogen at a standard rate of 7.57 slpm for places with a UV index > 11. Thermolysis of high salinity water is done by employing a solid oxide electrolyzer cell (SOEC), which comprises three customized, novel active optical subsystems to filter, track, and concentrate terrestrial UV solar irradiance by Fresnel lenses. The output of systems is fed to a desalinator, a photovoltaic system to produce electrical energy, and a steam generator with modified surface morphology to generate the required superheated steam for the SOEC. A simulation in COMSOL Multiphysics ver. 5.6 has shown that a customized honeycomb structure, when incorporated on the copper–nickel surface of a steam generator, improves its absorptance coefficient up to 93.43% (48.98%—flat case). This results in generating the required superheated steam of 650 °C with a designed active optical system comprising nine Fresnel lenses (7 m^2) that offer the concentration of 36 suns on the honeycomb structure of the steam generator as input. The required 1.27 kW of electrical power is obtained by concentrating the photovoltaic system using $In_{0.33}Ga_{0.67}N/Si/InN$ solar cells. This production of hydrogen is sustainable and cost effective, as the estimated cost over 5 years by the proposed system is 0.51 USD/kg, compared to the commercially available system, which costs 3.18 USD/kg.

Keywords: integration of renewable energy in industry; concentrated photovoltaics; solid oxide electrolyzer cells; thermolysis; honeycomb; absorptance coefficient

Citation: Butt, M.S.; Shahid, H.; Butt, F.A.; Farhat, I.; Sadaf, M.; Raashid, M.; Taha, A. Power Generation Analysis of Terrestrial Ultraviolet-Assisted Solid Oxide Electrolyzer Cell. *Energies* **2022**, *15*, 996. https://doi.org/10.3390/en15030996

Received: 8 December 2021
Accepted: 26 January 2022
Published: 28 January 2022

1. Introduction

The industrial revolution and evolving human lifestyles have resulted in a proportional increase in energy demand. Recently, it has been dealt with using conventional as well as renewable energy resources [1]. However, the exhaustive use of conventional or fossil fuel-based resources has created two problems. First, it leads to ozone depletion, and secondly, their usage causes disproportionate greenhouse gas emissions [2]. Among these, fluorinated gases, carbon dioxide, nitrous oxide, and methane pose a greater threat to the survival of the earth's ecosystem and have a larger impact on the air quality index. It is one of the major challenges of the researchers and policymakers of the 21st century [3,4]. To address the challenges faced by various regions of the earth due to air pollution, the World Health Organization (WHO), the United Nations Environment Program (UN Environment), and the World Meteorological Organization (WMO), with the support of the Climate and Clean Air Coalition (CCAC), are trying their best to deliver services in an integrated and

complementary manner to improve the air quality index. This will, in turn, improve the health and wellbeing of citizens worldwide [5]. At the same time, discovering or devising newer fuel types with the lowest carbon footprint to replace rapidly depleting fossil fuel energy sources has been declared another area of immense importance [6,7]. Energy generation via photovoltaics has been declared as one sustainable solution to both problems with the lowest carbon footprint [8]. Another method of energy generation via the utilization of hydrogen as a fuel has also been considered. For hydrogen production, systems already exist that employ the thermolysis of water [9,10]. This process uses xenon lamps as a light source and produces steam at 770 °C and 2 kW of electrical power to produce 8 slpm of hydrogen [11,12]. The terrestrial solar irradiance also contains UVA and UVB radiation but has never been used before for thermolysis, mainly due to their low percentage (~10%) of the solar spectrum reaching the earth [13,14] and health hazardousness.

In our study, we aimed to look at the possibility of employing terrestrial solar irradiance, UVA, and UVB (280 nm–400 nm) for the commencement of the thermolysis process. To overcome the problem of their lower intensities, an enhancement to a required level was achieved by using a light concentration mechanism with Fresnel lenses. Resultantly, the irradiance level was enhanced and aimed towards the surfaces of a solar panel, a desalinator, and a steam generator to fulfill the heat and electrical energy demands of water thermolysis for hydrogen generation. For the sake of providing the required electrical energy of a 1.27 kW concentrated photovoltaics (CPV) system with a conversion efficiency of 47% [15–17], $In_{0.33}Ga_{0.67}N/Si/InN$ tandem solar cells were used. To fulfill the 650 °C heat demand of the steam, a concept of light entrapment with the honeycomb structure, which was already established [18], was proposed to be employed for the proposed hydrogen generation system. Therefore, to enhance the absorption of concentrated and directed UVA and UVB radiation, a honeycomb structure was also incorporated on the surface of the steam generator [19,20].

This system finds its successful deployment for places where the UV index is >11, such as North America, Australia, New Zealand, Europe, and so forth [21]. It also renders the possibility of scaling up such individual systems along with their wireless integration throughout the world for places with a higher UV index to simultaneously operate wherever the UV index level requirement is achieved.

In this article, we discuss recent methods of light trapping in nanostructures to harness carbon-free green energy and modifications of these methods to suggest a novel design and implementation for UV entrapment for heat and electric power generation. The complete system was divided into subsystems, and each subsystem design was suggested and simulated in the respective software. A seamless system integration of the subsystem was proposed to generate hydrogen using only UV irradiation as a source.

2. Methods and Numerical Analysis

The proposed experimental setup was designed for the UV region of 280 nm–400 nm, which is ~10% of the solar irradiance spectrum. The total integrated power corresponding to this wavelength range is 41 W/m^2 [22,23], which is too low to directly fulfill the heat and electrical energy requirements for the commencement of a thermolysis process. Therefore, the concentration of UV irradiance needs to be enhanced. Here, this was done by designing three independent and customized novel optical systems based on the triple tracking of Fresnel lenses. The obtained concentrated UV irradiances were then used as input for the following three main subparts of the system:

- CPV
- Desalinator
- Steam generator

The schematic illustration of the proposed experimental setup is shown in Figure 1. It consists of three subsystems, including the desalinator, the steam generator, and the SOEC. Each of these subsystems receives concentrated UVA and UVB radiation of different intensities to provide the required output. Firstly, clean water from the desalinator is

supplied to the steam generator where it is heated by concentrated UVA and UVB radiation supplied by a customized active sun-tracking, filtering, and concentrating Fresnel lens system. The surface morphology of the steam generator is improved, which traps the concentrated irradiance inside and converts it easily into heat. This, in turn, heats the surface of the steam generator, and correspondingly, the thermal fluids inside of it (two-stage heating, discussed in Section 2.3). Resultantly, the generated steam is then fed to the SOEC, where the presence of the required electric power being provided by the UVA- and UVB-based CPV system initiates the thermolysis process. A continuous supply of desalinated water at the required rate is supplied under controlled pressure to obtain the required amount of hydrogen at a fixed rate of interest, 7.57 slpm. For the proposed experimental design and model, a steady-state analysis was performed to evaluate the performance of the system in comparison with the commercially available system.

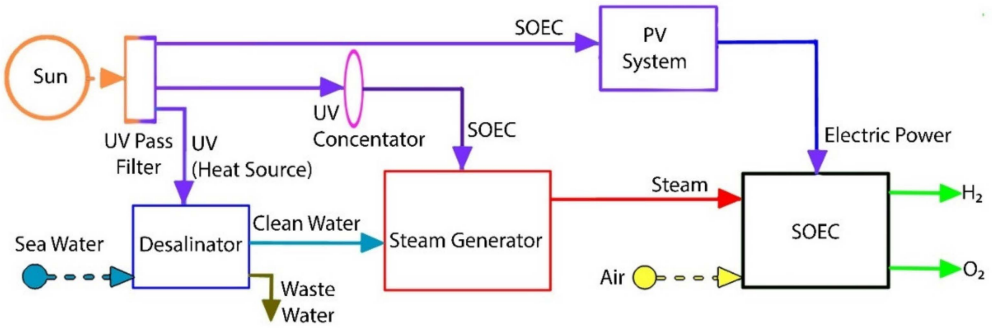

Figure 1. Block diagram of the proposed experimental setup with three subparts: desalinator, CPV system, and team generator. Each of these is supplied by concentrated UVA and UVB obtained from an optically active Fresnel lens array. SOEC is fed by superheated steam at 650 °C.

The overall research framework of the proposed experimental setup and methodology in the form of a schematic is shown in Figure 2.

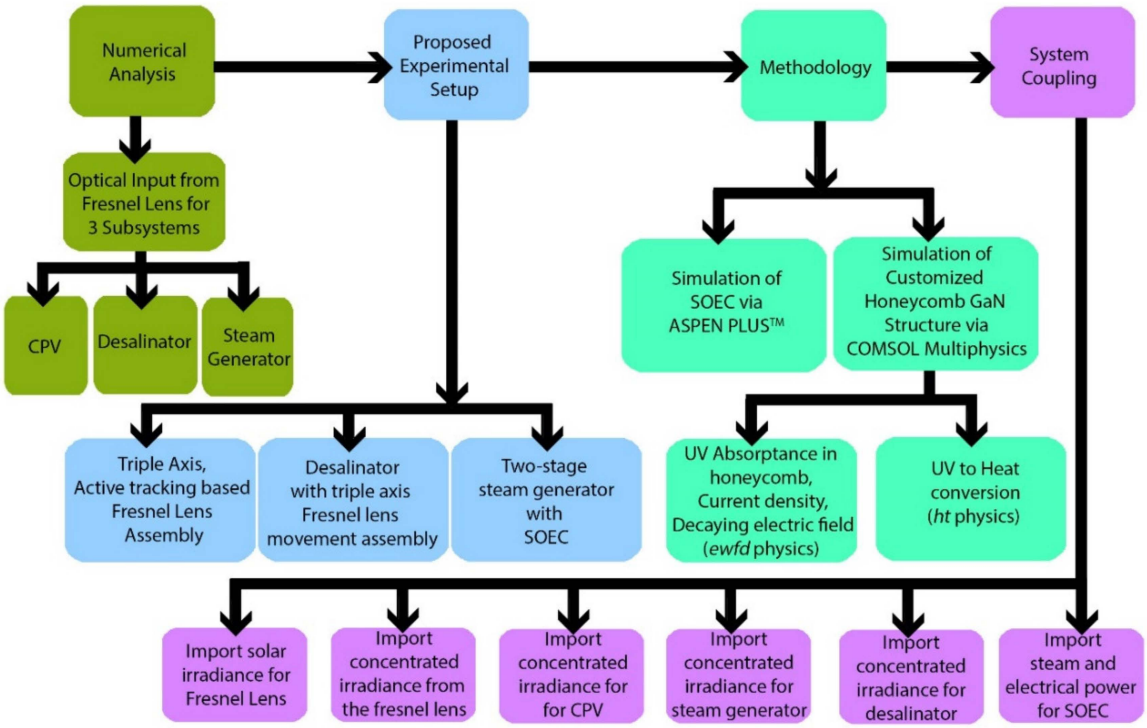

Figure 2. The schematic framework of the overall research of this paper.

2.1. CPV System Design for Electrical Energy Generation

The PV system designed for the proposed system is an actively stabilized solar irradiance CPV system that provides the required electrical energy for the thermolysis process. The overall system comprises a Fresnel lens and PV cell array, as shown in Figure 3a. The lens firstly aligns with the sun to receive maximum radiation, and then the lateral movement of the lens adjusts the irradiance intensity to a reference value of interest over the PV cell array. This allows the proposed system to provide a fixed 1.27 kW for cases when the UV index is >11 during the sun hours specified for a certain country. The technical specifications of the active optical UV irradiance collector and the concentration system are given in Table 1

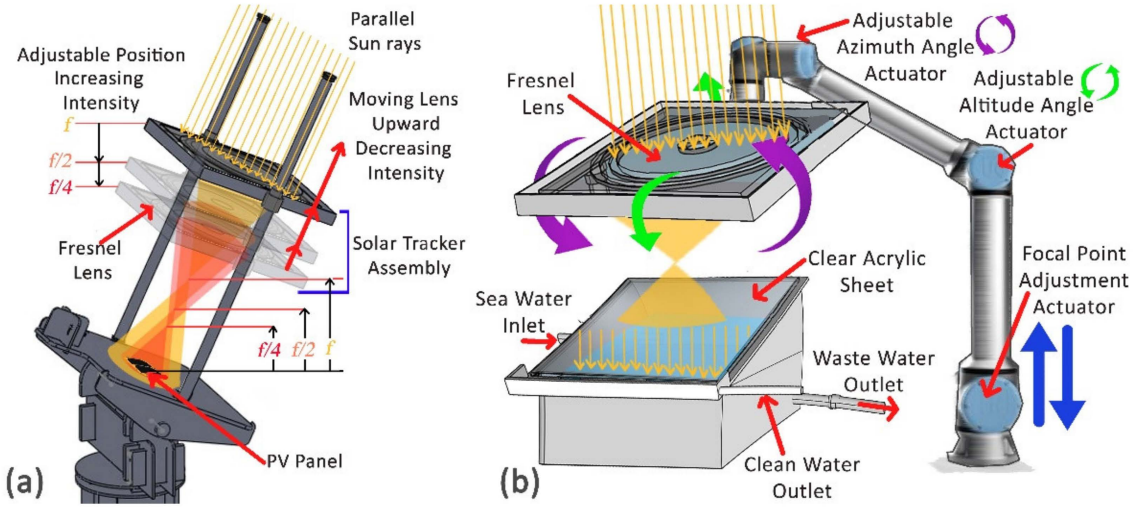

Figure 3. (**a**) An active Fresnel lens concentrating UVA and UVB (280 nm–400 nm) at PV panel by adjusting its focal point. When solar irradiance decreases, re-positioning of the lens takes place to adjust the spot size to keep the fixed value of solar interest. (**b**) Proposed desalinator structure with triple-axis Fresnel lens movement assembly for tracking the sun, filtering, and concentrating UVA and UVB (280 nm to 400 nm), and temperature adjustment to maintain 120 °C inside the water tank.

Table 1. Proposed design specifications of Fresnel lens concentrator for CPV system.

Design Parameters	Description
Circular solar concentrator lens area with UV pass filter	0.565 m^2
Maximum electric power	1.3 kW
Maximum temperature	70 °C
Focal length	1.5 m
Spot diameter	0.0034 m^2
Concentration ratio	147

Perovskite materials, with a 27.3% efficiency, are cost-effective candidates to be used as solar cells [24]. The performance of multijunction perovskite cells exhibits better efficiency and stability at 30.7% [25]. However, GaN-based photovoltaics are normally fabricated on sapphire (Al_2O_3) substrates, but due to the higher cost of the substrate, low thermal conductivity, and unavailability in large diameters, Si is considered an alternative [26]. In addition, in typical $InxGa_{1-x}N$, the indium content of $InxGa_{1-x}N$ alloys cannot exceed 33%, and its conversion efficiency cannot exceed 28% [27]. On the other hand, it is reported that an efficiency greater than 40% can be achieved by introducing a silicon sub-cell in tandem cell configurations. The two sub-cell $In_{0.33}Ga_{0.67}N/Si$ system presents an efficiency of 42.43%, and the three sub-cell $In_{0.33}Ga_{0.67}N/Si/InN$ system gives a 47.83% efficiency under one-sun radiation. Considering the III-nitride-based material, three sub-cell $In_{0.33}Ga_{0.67}N/Si/InN$ system can be used with the maximum conversion efficiency

of 47.83% and covers almost the entire solar spectrum (0.7 eV–3.4 eV) [28]. Therefore, $In_{0.33}Ga_{0.67}N/Si/InN$ is more cost effective considering its additive advantage of higher efficiency than a single junction silicon module and a perovskite silicon double junction module. Therefore, an $In_{0.33}Ga_{0.67}N/Si/InN$ solar array comprising 385 cells (0.1 cm^2 area of 1 cell) was proposed to be used to generate the required electrical energy of 1.27 kW (the SOEC system electrical energy requirement) by using concentrated UVA and UVB radiation and incorporating a triple-axis solar tracker, as shown in Figure 3a. This is a modified CPV technology. In the case of the solar tracker, the proposed experimental setup uses UVA and UVB (280 nm–400 nm) radiation bands from the sunlight as input to a Fresnel lens. A light funnel is formed along its focal length, exhibiting varying light intensities along its axial direction on the underside. On the surface of the PV cell, the input light intensity-dependent axial movement of this light funnel controls the UV solar irradiance intensity. By using triple-axis tracking control, the optimum irradiance on the panel surface is achieved. Firstly, dual-axis tracking control for the panel movement, and secondly, axial movement control for the lens is provided. The proposed experimental setup takes the corresponding value of solar irradiance on the solar array as a reference value and maintains it via light intensity-dependent axial movement of the light funnel created by the Fresnel lens. For the cases where spot irradiance varies during different hours of the day, with clouds, or in conditions when solar irradiance is changed, the system employs optimized triple-axis tracking and adjusts the lens position accordingly. By doing this, the light funnel moves upwards or downwards along with the lens in the axial direction so that the spot irradiance adjusts itself, aiming for the reference value. In this way, the output power is kept fixed at the value of interest.

2.2. Design of the Desalinator for the Generation of Pure Water for the Steam Generator

The optical structures consisting of a single Fresnel lens with a surface area of 0.16 m^2 to obtain concentrated light for the purpose of desalination are shown in Figure 3b. The assembly consists of a triple-axis solar tracking mechanism that moves the Fresnel lens to adjust the water temperature. A robotic arm structure was proposed that can move the Fresnel lens along three axes. A focal point adjustment actuator is a linear actuator motor that can shift the focal point of the lens assembly to the spot size, and thus, it can increase or decrease the intensity of the incident rays striking the surface of the water. An adjustable altitude angle actuator is a stepper motor that can lock the sun rays orthogonal to the surface of the lens, and hence, it can track the sun's altitude angle from east to west. An adjustable azimuth angle actuator is a stepper motor that will adjust the tilt angle of the lens assembly to the declination angle so that the sun rays strike the collector at the best possible angle. The lens sheet first gets aligned with the sun to receive the maximum radiation and then, by its lateral movement, the irradiance intensity is adjusted to the desired value of the temperature of the water. These rays directly heat the water to 120 °C and allow the proposed system to operate at 70 J/s.

The desalinator for the proposed project was designed with a water inflow rate of 1 kg/h. A tank with dimensions of 0.4 × 0.4 m^2 and 0.2 m of height is used to store 1 kg of seawater. An acrylic glass sheet was incorporated for providing a gravitational effect to the condensed water vapors that travel to the distilled water tank. Saltwater is taken to another tank, where 0.5 kg/h of desalinated water is produced to fulfill the steam generation requirements. The water temperature inside the tank is maintained at a maximum of 120 °C to avoid excessive steaming. With 41 W/m^2 of UV as an irradiation input, the overall system requirements are fulfilled by 70 J/s of power, including a 20% safety margin.

2.3. Design of the UV Light Entrapment with Honeycomb Structure for the Steam Generator

The pretreated water from the desalinator is transferred to a steam generator made of Cu–Ni composite material, providing high mechanical strength and temperature endurance. Owing to the reflecting nature of the plain Cu–Ni surface of the steam generator,

for obtaining superheated steam of the required temperature with UV light, the proposed design suggests an improvement in the surface morphology of the steam generator via incorporating a honeycomb structure on its outer surface. This assists in the entrapment of the UV light, which will, in turn, result in heat generation at the surface of the steam generator to obtain the superheated steam of the required temperature inside of it. Therefore, an optimized honeycomb structured layer of GaN was proposed to be incorporated with Cu–Ni to maximize the absorptance of UV concentrated on it. The simulation findings verify the theoretical analysis that UV gets trapped in the structure, resulting in an enhanced radiation absorptance in comparison to a flat reflecting surface of the steam generator. This in turn results in the conversion of the UV electromagnetic radiation to heat at the external surface of the steam generator. This heat then gets transferred inside the DOWTHERMTM oil and then to the molten carbonates to achieve temperatures up to 350 °C and 650 °C, respectively, via the two-stage heating process required for the SOEC operation initiation. The proposed two-stage design of the steam generator is shown in Figure 4. The design parameters of the steam generator design are listed in Table 2.

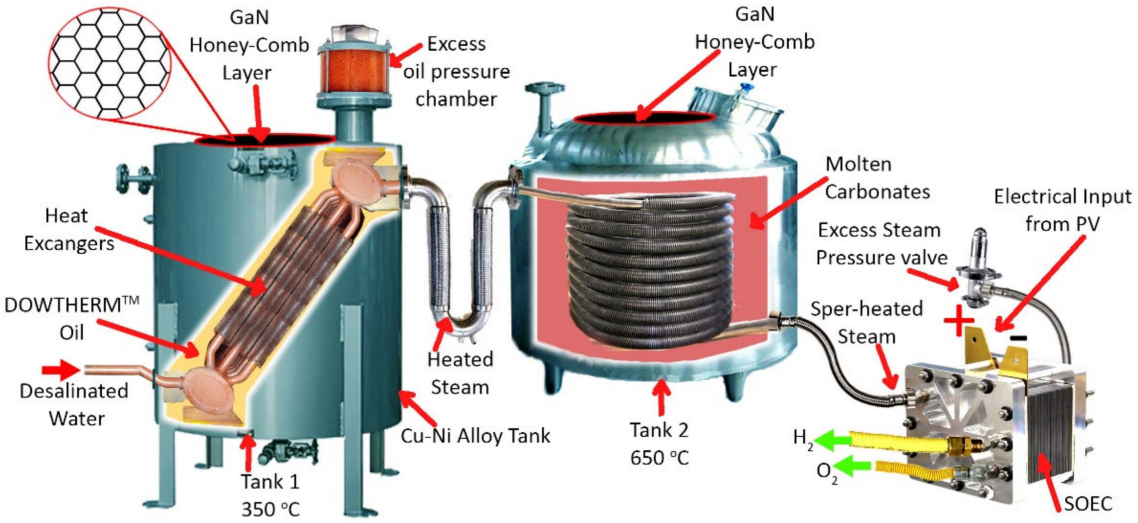

Figure 4. The proposed assembly of the steam generator and SOEC; inputs are desalinated water and electrical power from PV, outputs are hydrogen and oxygen; GaN honeycomb structure is present at the top of Tank 1 and Tank 2.

Table 2. Proposed steam generator design specifications.

Technical Specifications	Description
Vessel	High-quality copper–nickel alloy
Thermal conductivity	70 W/mK at 1000 °C
Maximum thermal power	(Honeycomb effect include)
Heat transfer fluids	DOWTHERM^{TM} oil (350 °C Max)
Steam generator	Molten carbonates (650 °C)
Steam tubes material	SS 304 pressure tubing
Ambient temperature	25 °C
Dimension	1 × 1 m^2
Thickness	1.5 cm
Water flow rate	0.5 kg/h

The honeycomb structure's optimized design parameters used for simulation purposes are provided in Table 3.

Table 3. Design parameters of the honeycomb structure incorporated into the steam generator.

Technical Data	Description
Honeycomb material	GaN
GaN outer axial length	400 nm
GaN inner hole depth	300 nm
Fill factor (FF)	0.505
Lattice constant (diagonal length)	400 nm
Diameter of nanohole (reference diameter)	256 nm
Structure simulated in 5 steps for hole diameter	160 nm to 336 nm

The required input UV light concentration is suggested to be obtained with a customized Fresnel lens triple-axis tracking mechanism installed outside of the Cu–Ni surface of the steam generator. For this purpose, the technical specifications of the concentrating optics comprising the Fresnel lenses array are given in Table 4.

Table 4. Proposed design specifications of Fresnel lens concentrator for steam generation.

Design Parameters	Description
Circular solar concentrator lens area with UV pass filter	7 m^2 (assembly of 9 lenses, 1 m^2 area each)
Minimum temperature	650 °C
Spot diameter	0.0063 m^2
Maximum concentration	1100

This steam enters the SOEC stack, where electrolysis takes place. The electrolyzer was designed to operate at thermoneutral voltage to obtain the highest electricity-to-fuel efficiency. The electrical and thermal energy required to operate the electrolyzer at thermoneutral voltage is obtained from the PV system and an active optical structure, respectively.

The SOEC consists of a cathode, an electrolyte, and an anode used to generate hydrogen and oxygen. The oxide ions produced at the cathode move towards the anode through electrolytes, that is, yttria-stabilized zirconia (YSZ). The electrons generated at the anode then flow through the external circuit towards the cathode to close the circuit [29–31]. The whole experimental setup, including the steam generator and the SOEC, was simulated in the process simulation tool ASPEN PLUS^{TM} using the available heater, reactor, separator, mixer, and splitter models.

3. Results

3.1. UV Absorptance Improvement Due to Honeycomb Structure

The UV's maximum absorptance coefficient occurred when the hole diameter was between the range of 200 nm and 300 nm [18]. The data in Figure 5 inset depict that the GaN nanohole of the hexagonal array had better UV (280 nm–400 nm) absorption performance with a lattice constant (diagonal dimensions) of 400 nm. The hole diameter varied from 160 nm to 336 nm, that is, had values of 160 nm, 200 nm, 256 nm, 300 nm, and 330 nm. The simulated results of the UV absorptance co-efficient against the UV radiation (280 nm–400 nm, with an incremental step size of 20 nm) irradiated on the GaN honeycomb structure with a hole diameter of 256 nm are presented in Figure 5. These findings were further extended to simulate the GaN honeycomb structure on the 300 nm layer of Cu–Ni composite to observe the difference in absorptance due to the presence of the Cu–Ni composite layer. The results are shown in Figure 5, and it is evident that the shiny metallic surface of the Cu–Ni composite reflected an average of 54.02% of incident UV (36.56% at 280 nm and 71.48% at 400 nm). The GaN honeycomb structure increased the absorptance coefficient of the UV to 93.43%. This difference in absorption (47.45%) is utilized to harness heat energy from UV radiation.

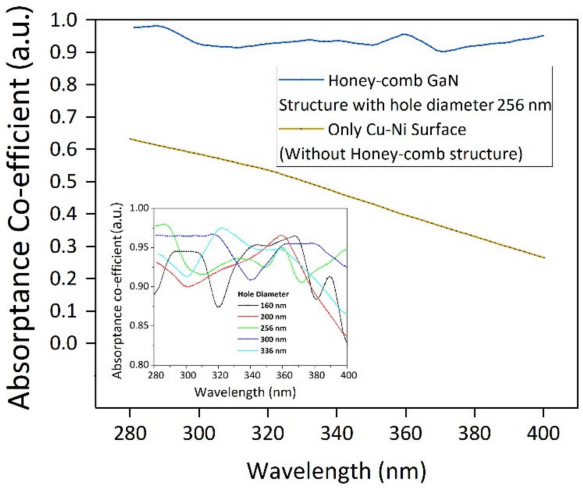

Figure 5. Graph presenting absorptance coefficient of Cu–Ni layer with and without honeycomb GaN structure against UV irradiance. The inset presents absorptance of UV at different hole diameters.

3.2. Current Density Distribution in the Honeycomb Structure

A single honeycomb structure was simulated with the periodic conditions to limit the simulation time in COMSOL. The mesh size was set to "extremely fine" along with "free tetrahedral" mesh, which was superimposed to precisely simulate this model at an arc length of a maximum of 600 nm. The honeycomb structure was irradiated with UVA and UVB with a parametric sweep step size of 24 nm. A surface current density of 1×10^9 A/m^2 in this nanostructure was observed from the simulations, and the results are presented in Figure 6a. This current density produces 10 nW of power loss in a single honeycomb structure when taking the inner walls, outer walls, inner hole, and top surface into account by calculating the material resistivity of GaN (resistivity at 650 °C = 1×10^9 Ω.m). The increased absorptance observed from Figure 5 indicates that this UV absorptance in honeycomb structures can create electric power loss to produce heat.

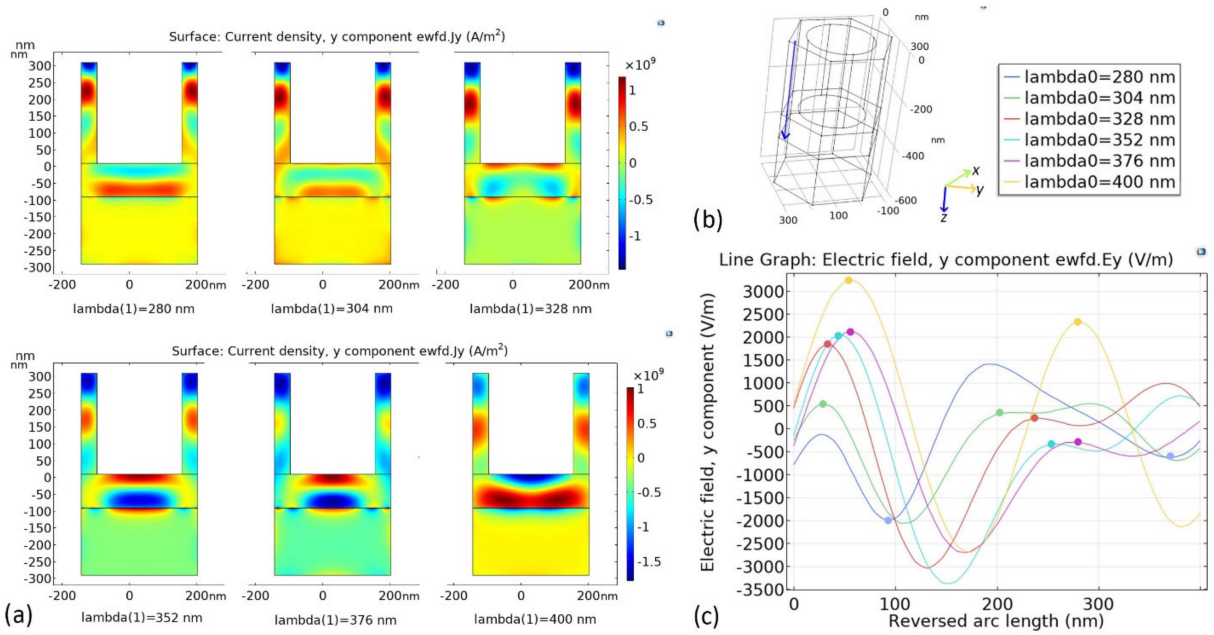

Figure 6. (**a**) Surface current density at the half-cut plane of single honeycomb hexagon at different wavelengths. (**b**) Blue line presents reverse arc length (path of decaying electric field). (**c**) Line plot of decaying electric field (V/m) as a function of reverse arc length presenting absorptance of UV irradiance in honeycomb GaN structure.

3.3. Electric Field and Power Dissipation in a Honeycomb Structure

Another aspect of UV absorptance in the nanohole honeycomb structure was simulated to obtain the electric field plot against the reverse arc length in the negative z-axis, as shown in Figure 6b. A decaying UV waveform can be observed in Figure 6c when the UV penetrated the sidewalls of the honeycomb structure. The plot shown in Figure 6c was obtained by applying electromagnetic waves, frequency domain (ewfd) physics interface (COMSOL) given by Equation (1)

$$\nabla \times \mu_r^{-1}(\nabla \times E) - k_O^2\left(\epsilon_r - \frac{j\sigma}{\omega\epsilon_o}\right)E = 0 \quad (1)$$

The electric field obtained from the simulation results has a relation presented in damped sinewave Equation (2) and was acquired by using a curve-fitting tool. To calculate the decay of the electric field, an approximation was done and it was assumed that there was no change in the incident wavelength of the UV.

$$Ey(t) = A \times e^{-\lambda t}(\cos(\omega t + \varphi)) \quad (2)$$

where λ is the decaying constant. The decay coefficient for the incident UV wavelength was calculated from the sine wave in Figure 6c considering two consecutive positive or negative peaks of the electric field curve as (A_1, A_2) and their respective projections as (x_1, x_2) by substituting these numerical values in slope Equation (3), as follows:

$$\text{projection} = \frac{A_1 \,/\, A_2}{x_2 - x_1} \quad (3)$$

An arbitrary power loss distribution of coefficient (2λ) was obtained from the average intensity Equation (4), where I_{avg} is the intensity of incident UV in W/m^2.

$$I_{avg} = \frac{c\epsilon_o E_o^2}{2}\left(\frac{W}{m^2}\right) \quad (4)$$

Figure 7 represents the power loss distribution (2λ) for different wavelengths, and the maximum heat dissipation was observed at 320 nm to 380 nm, which is a high proportion of the UV in the solar irradiance spectrum.

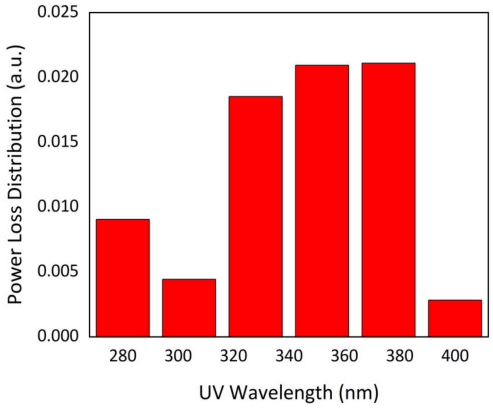

Figure 7. Calculated results from the simulated data of the electric field are presented in the power loss distribution plot for different wavelengths of incident UV.

3.4. UV to Heat Conversion

It is evident from the above calculations that increased UV absorption led to additional power losses in the honeycomb GaN structure and, therefore, generated more heat energy from incident electromagnetic radiation. This added heat energy generation can

be attributed to the structural and material properties of GaN. Another simulation was employed to calculate the temperature requirement for the system to produce super-heated steam for thermolysis. A 3 × 3 matrix of the honeycomb structure is shown Figure 8a for this purpose and was tested with the mathematical equations from the simulation solver, Equations (5) and (6), with the physics set to heat transfer in solids (*ht*).

$$\rho C_p u \times \nabla \times q = Q + Q_{ted} \quad (5)$$

$$q = -k\nabla T \quad (6)$$

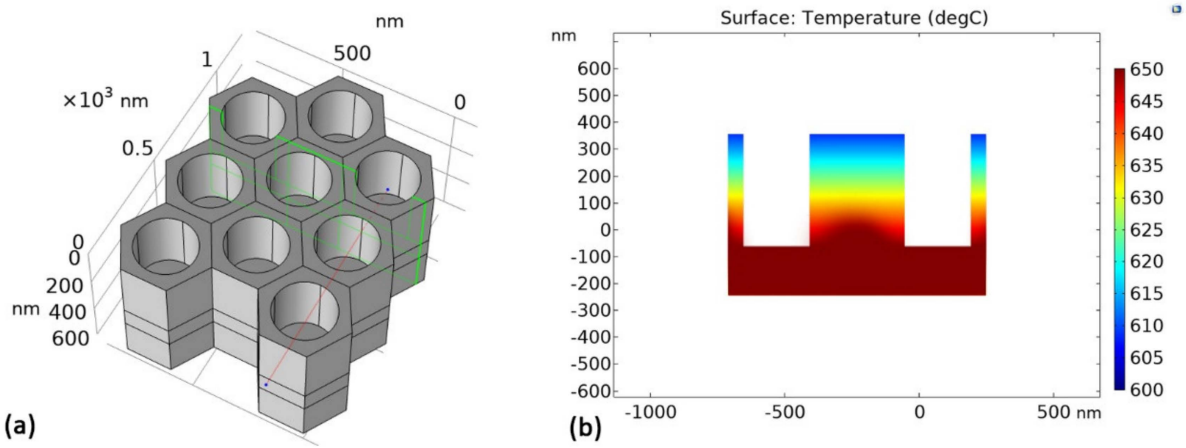

Figure 8. (**a**) Cut plane of honeycomb hexagonal structure along *z*-axis presented by green surface. (**b**) Internal surface temperature distribution in °C of honeycomb along the *z*-axis from GaN to Cu–Ni alloy layer.

The mesh size was set to the "extremely fine" configuration and the boundary conditions were set at "periodic" to simulate a wide layer of honeycomb structure for a concentrated UV spot size (63.59 cm^2). The temperatures of 650 °C, 600 °C, and 615 °C were obtained at the lower surface of Cu–Ni, the middle layer of GaN, and the top layer, respectively. The decrease in temperature at the top layer was due to its heat dissipation in the ambient environment. Figure 8 shows the inward flow of heat from the GaN layer to the Cu–Ni alloy steam container by considering the cut plane of the simulated model.

4. Discussions

4.1. Steam Generation, Electrolysis, and Hydrogen Production

The superheated steam obtained from the steam generator "STM-GEN" was mixed with the hydrogen gas and recycled from the cathode exhaust (stream RECIR-H2) to prevent the oxidation of the cathode material. The RSTOIC model, represented by CATHODE, simulated the steam electrolysis reaction with SOEC operating conditions. The steam utilization factor was defined by the reaction conversion in the CATHODE block settings. Since the SOEC requires electrical and thermal energies to carry out the electrochemical reactions, the electrical energy (represented by POWER) and thermal energy (represented by HEAT) were supplied from external sources. Both the POWER and HEAT were calculated by mathematical coding equations, given in Table 5, in the calculator block (CALC). Oxygen was first separated from the hydrogen and unreacted steam in the separator block (ELECTROL), and then mixed with air at the anode (ANODE) to simulate the SOEC anode electrode. The products of the cathode electrode (stream FH2H2O) were partially recycled to provide the desired steam-to-hydrogen ratio remaining withdrawn from the system. The steam-to-hydrogen ratio was adjusted using the Design Spec feature of Aspen Plus.

Table 5. Summary of mathematical equations coded in the CALC block of Aspen Plus.

Parameter	Expression
Equilibrium voltage (E)	$E = E_0 - \frac{RT}{nF} \ln\left(\frac{P_{H_2} P_{O_2}^{0.5}}{P_{H_2}}\right)$ where $E_0 = 1.253 - 2.451.10^{-4}T$
Cell voltage (Vcell)	$V_{cell} = E + ASR \cdot i$
Area-specific resistance (ASR)	$ASR(T,P) = 35.51 \exp(-0.0058T) \exp(-0.0217P)$
Current density (i)	$i = \frac{4F \cdot n_{O_2}}{N_{cell} \cdot A_{cell}}$
Electrical power required (Pstack)	$P_{stack} = i \cdot V \cdot N_{cell} \cdot A_{cell}$

Table 6 presents the simulation results of the steam generation and electrolysis. It can be observed that the steam generation at 10.4 slpm required 0.50 kW of thermal power, which was supplied from the concentrated UV radiation. The steam required 1.27 kW of electrical power and 0.17 kW of thermal power for steady-state operation to feed an SOEC stack comprising 22 cells, with each electrode active area of 100 cm^2 requiring 1.27 kW of electrical power and 0.17 kW of thermal power for steady-state operation. The SOEC stack then produced hydrogen at a rate of 7.57 slpm. These values agree with those in the reported literature, where 8 slpm of H_2 was produced. The lower value (7.57 slpm) of the proposed system was due to the lower working temperature, that is, 650 °C, compared to the temperature of 770 °C in the referenced system [19].

Table 6. Steam generator and SOEC simulation result in ASPEN Plus.

Parameter	Value	Unit
Steam generator		
Temperature	650	°C
Pressure	1.5	Bar
Steam generation rate	10.4	Slpm
Thermal power required	0.50	kW
SOEC Stack		
Operating temperature	650	°C
Operating pressure	1.5	Bar
Steam utilization factor	0.7	-
Unit cell active area	100	cm^2
Number of cells in the stack	22	-
Cell voltage	1.17	V
Hydrogen production rate	7.57	Slpm
Electrical power required	1.27	kW
Thermal power required	0.12	kW

4.2. Model Validation

The model explained in Section 3.1 shows the absorption of UV on the honeycomb structure. This is in agreement with the reference research article [24], where the model showed the maximum absorptance of UV set at a nanohole diameter of 256 nm. Taking this value as a reference, the model was further analyzed at different UV wavelengths, and the data were further processed under the electromagnetic waves and frequency domain interface in COMSOL. The model converts electromagnetic waves to heat with maximum efficiency. The study in [18] investigated the efficient light-trapping phenomenon in nanostructures. Our system utilized this study to implement a complete system that generates hydrogen at a cheaper cost, as explained in Section 4.3. This is a novel approach integrating recent studies to make a complete system that can generate hydrogen using sustainable energy sources.

4.3. Cost Analysis of the Proposed System

Considering the 2021 wind and solar costs, most of the planned green hydrogen projects will end up with a hydrogen selling price between USD 3.18 and USD 5.75 per kg [32]. The costs of the proposed systems were calculated for a period of 5 years. The individual costs of the equipment suggested are presented in Table 7.

Table 7. The individual costs of components in the proposed system.

Equipment Detail	Price (USD)	Number of Units	Total Price (USD)
$In_{0.33}Ga_{0.67}N$/Si/InN PV cell	150	385	38,500
Fresnel lens (1 m^2)	250	12	2400
Triple-axis active solar tracker assembly	1000	4	3000
SOEC Stack	800	22	17,600
Steam generator	1500	2	2000
GaN honeycomb layer assembly	1000	2	1000
Desalination system	1000	1	1000
UV filter	500	4	900
Integration of equipment	2000	1	2000
Hydrogen storage cost	2000	1	5000
Maintenance cost over 5 years	10,000	1	5000
Running cost over 5 years	20,000	1	20,000
Total cost of equipment	——	436	124,350

The proposed system can produce 7.57 slpm of hydrogen, which is equivalent to 32.15 kg/h. Considering an average of 5 h of daylight per day in a year, the production of hydrogen that can be acquired in 5 years is 296 mt. If the total equipment cost, installments, depreciation, and human resources are calculated to be 150,000 USD, then the acquired yield of hydrogen would be 0.51 USD. It is cheaper than the commercially available hydrogen and has the additional advantage of sustainable production as well.

5. Conclusions

An active, efficient, cost-effective, and self-sustaining system was designed and simulated to utilize solar radiation (UVA and UVB) to produce H_2 through an SOEC. The designed system comprises three subsystems (a desalinator, a steam generator, and an SOEC). UVA and UVB irradiance are used to produce the thermal power needed for the operation of the desalinator and steam generator. The electrical power required for the SOEC is attained by irradiating the CPV system with UV radiation. The active optical systems, with an array of Fresnel lenses accompanied with active solar trackers, were employed to obtain concentrated UV radiation. Clean water is obtained by the desalinator using the concentrated UV radiation. A nanostructure of GaN, in a customized honeycomb shape that has an improved UV absorptance coefficient (~93.43%), is employed to generate superheated steam from the clean water. The nanostructure was simulated and carefully analyzed to calculate the heat-generating capacity of the UV irradiation. The generated steam was then utilized in the SOEC to obtain H_2 through the thermolysis process. The designed system, along with the subsystems, yielded better output compared to that already reported in the literature. The complete system was also simulated and modeled as a single system by performing design calculations on the UV irradiance conversion to electric and thermal power. The results of both the reported literature and the simulations confirm that the designed system is a cost-effective and efficient system to produce hydrogen using only UV radiation. The system has sustainable production capabilities if such systems are installed all over the world with an integrated operation to ensure 24 h supply and initiating generation wherever the UV index reaches 11 or higher. The environmental impact of this system is very high for improving the air quality and can be considered in further studies.

Author Contributions: Conceptualization, H.S. and M.S.B.; methodology, H.S. and M.S.B.; software, F.A.B.; validation, M.S.B. and I.F.; formal analysis, M.S.; investigation, M.R.; writing—original draft preparation, M.S.B.; writing—review and editing, A.T. and M.S.B.; supervision, H.S.; project administration, H.S. and M.S.B.; funding acquisition, A.T. All authors have read and agreed to the published version of the manuscript.

Funding: This study was supported in part by the Engineering and Physical Sciences Research Council (EPSRC) Grants, EP/T517896/1.

Institutional Review Board Statement: Not applicable.

Informed Consent Statement: Not applicable.

Data Availability Statement: Not applicable.

Acknowledgments: This study was supported in part by the Engineering and Physical Sciences Research Council (EPSRC) Grants, EP/T517896/1. All authors have consented to the acknowledgement.

Conflicts of Interest: The authors confirm that this manuscript has no conflict of interest.

Abbreviations

UV	Ultraviolet
SOEC	Solid oxide electrolyzer cell
GaN	Gallium nitride
WHO	World Health Organization
WMO	World Meteorological Organization
CCAC	Climate and Clean Air Coalition
CPV	Concentrated photovoltaics
Slpm	Standard liter per minute
YSZ	Yttria-stabilized zirconia
E	Electric field (V/m)
M	Permeability (H/m)
ϵ	Permittivity (F/m)
λ	Decaying constant
I_{avg}	Average intensity (W/m^2)
Cp	Specific heat capacity at constant pressure (J/(kg·K))
Q	Heat source (W/m^3)
$(\rho C_p)_{eff}$	Effective volumetric heat capacity at constant pressure ($J/(m^3 \cdot K)$)

References

1. Sher, F.; Curnick, O.; Azizan, M.T. Sustainable conversion of renewable energy sources. *Sustainability* **2021**, *13*, 2940. [CrossRef]
2. Panchasara, H.; Samrat, N.H.; Islam, N. Greenhouse gas emissions trends and mitigation measures in australian agriculture sector—A review. *Agriculture* **2021**, *11*, 85. [CrossRef]
3. Irshad, M.; Khalid, M.; Rafique, M.; Tabish, A.N.; Shakeel, A.; Siraj, K.; Ghaffar, A.; Raza, R.; Ahsan, M.; Tul Ain, Q.; et al. Electrochemical investigations of bace0.7-xsmxzr0.2y0.1o3-δ sintered at a low sintering temperature as a perovskite electrolyte for it-sofcs. *Sustainability* **2021**, *13*, 12595. [CrossRef]
4. Sokka, L.; Sinkko, T.; Holma, A.; Manninen, K.; Pasanen, K.; Rantala, M.; Leskinen, P. Environmental impacts of the national renewable energy targets—A case study from Finland. *Renew. Sustain. Energy Rev.* **2016**, *59*, 1599–1610. [CrossRef]
5. World Health Organisation. *Delivering on Air Quality, Climate Change and Health*; World Health Organisation: Geneva, Switzerland, 2016; pp. 1–6.
6. Gazda-Grzywacz, M.; Winconek, Ł.; Burmistrz, P. Carbon footprint for mercury capture from coal-fired boiler flue gas. *Energies* **2021**, *14*, 3844. [CrossRef]
7. Guo, Y.; Pan, Z.; An, L. Carbon-free sustainable energy technology: Direct ammonia fuel cells. *J. Power Sources* **2020**, *476*, 228454. [CrossRef]
8. Tawalbeh, M.; Al-Othman, A.; Kafiah, F.; Abdelsalam, E.; Almomani, F.; Alkasrawi, M. Environmental impacts of solar photovoltaic systems: A critical review of recent progress and future outlook. *Sci. Total Environ.* **2021**, *759*, 143528. [CrossRef]
9. Daneshpour, R.; Mehrpooya, M. Design and optimization of a combined solar thermophotovoltaic power generation and solid oxide electrolyser for hydrogen production. *Energy Convers. Manag.* **2018**, *176*, 274–286. [CrossRef]
10. Huang, W.; Hu, G.; Tian, C.; Wang, X.; Tu, J.; Cao, Y.; Zhang, K. Nature-inspired salt resistant polypyrrole-wood for highly efficient solar steam generation. *Sustain. Energy Fuels* **2019**, *3*, 3000–3008. [CrossRef]

11. Hosseini, S.E.; Wahid, M.A. Hydrogen from solar energy, a clean energy carrier from a sustainable source of energy. *Int. J. Energy Res.* **2020**, *44*, 4110–4131. [CrossRef]
12. Elgeziry, M.; Hatem, T. Designing a Dual-axis Open-loop solar tracker for CPV applications. In Proceedings of the 47th IEEE Photovoltaic Specialists Conference (PVSC), Calgary, AB, Canada, 15 June–21 August 2020; pp. 1522–1524. [CrossRef]
13. Häder, D.P.; Barnes, P.W. Comparing the impacts of climate change on the responses and linkages between terrestrial and aquatic ecosystems. *Sci. Total Environ.* **2019**, *682*, 239–246. [CrossRef]
14. Zhu, T.; Li, Q. A novel spectrum allocation method in the photovoltaic-thermochemical hybrid solar system. *J. Power Sources* **2021**, *513*, 230541. [CrossRef]
15. Shahid, H.; Kamran, M.; Mehmood, Z.; Saleem, M.Y.; Mudassar, M.; Haider, K. Implementation of the novel temperature controller and incremental conductance MPPT algorithm for indoor photovoltaic system. *Sol. Energy* **2018**, *163*, 235–242. [CrossRef]
16. Rejeb, O.; Shittu, S.; Ghenai, C.; Li, G.; Zhao, X.; Bettayeb, M. Optimization and performance analysis of a solar concentrated photovoltaic-thermoelectric (CPV-TE) hybrid system. *Renew. Energy* **2020**, *152*, 1342–1353. [CrossRef]
17. Burhan, M.; Shahzad, M.W.; Oh, S.J.; Ng, K.C. A pathway for sustainable conversion of sunlight to hydrogen using proposed compact CPV system. *Energy Convers. Manag.* **2018**, *165*, 102–112. [CrossRef]
18. Zhangyang, X.; Liu, L.; Lv, Z.; Lu, F.; Tian, J. Efficient light trapping in GaN inclined nanorod and nanohole arrays for photocathode applications. *Opt. Mater.* **2020**, *101*, 109747. [CrossRef]
19. Schiller, G.; Lang, M.; Szabo, P.; Monnerie, N.; von Storch, H.; Reinhold, J.; Sundarraj, P. Solar heat integrated solid oxide steam electrolysis for highly efficient hydrogen production. *J. Power Sources* **2019**, *416*, 72–78. [CrossRef]
20. Jagadish, R.; Malar, P. Surface texturing of Cu2ZnSnSe4 thin films for enhanced optical absorbance. *Sol. Energy* **2020**, *201*, 387–397. [CrossRef]
21. Downs, N.; Parisi, A.V.; Galligan, L.; Turner, J.; Amar, A.; King, R.; Ultra, F.; Butler, H. Solar radiation and the uv index: An application of numerical integration, trigonometric functions, online education and the modelling process. *Int. J. Res. Educ. Sci.* **2016**, *2*, 179–189. [CrossRef]
22. Rizescu, D.; Rizescu, C.I.; Alionte, C.G. Researches on the development of an optical system for improving the efficiency of photovoltaic panels. *E3S Web Conf.* **2020**, *180*, 02008. [CrossRef]
23. Pham, T.T.; Vu, N.H.; Shin, S. Novel design of primary optical elements based on a linear fresnel lens for concentrator photovoltaic technology. *Energies* **2019**, *12*, 1209. [CrossRef]
24. Hossain, M.I.; Qarony, W.; Ma, S.; Zeng, L.; Knipp, D.; Tsang, Y.H. Perovskite/Silicon Tandem Solar Cells: From Detailed Balance Limit Calculations to Photon Management. *Nano-Micro Lett.* **2019**, *11*, 58. [CrossRef]
25. Paper, C.; Bombay, T.; Bombay, T. Future Prospects of InGaN/GaN Multiple Quantum Well Solar Cells Research for High Quantum Efficiency and Cost Effectiveness Future Prospects of InGaN/GaN Multiple Quantum Well Solar Cells Research for High Quantum Efficiency and Cost. 2012. Available online: https://www.researchgate.net/publication/263440797_Future_prospects_of_InGaNGaN_Multiple_Quantum_Well_Solar_Cells_Research_for_High_Quantum_Efficiency_and_Cost_effectiveness (accessed on 11 November 2021).
26. Wang, Z.; Song, Z.; Yan, Y.; Liu, S.F.; Yang, D. Perovskite—A Perfect Top Cell for Tandem Devices to Break the S–Q Limit. *Adv. Sci.* **2019**, *6*, 1801704. [CrossRef] [PubMed]
27. Nguyen, T.T.; Patel, M.; Kim, S.; Mir, R.A.; Yi, J.; Dao, V.A.; Kim, J. Transparent photovoltaic cells and self-powered photodetectors by TiO2/NiO heterojunction. *J. Power Sources* **2021**, *481*, 228865. [CrossRef]
28. Roghabadi, F.A.; Fumani, N.M.R.; Alidaei, M.; Ahmadi, V.; Sadrameli, S.M. High Power UV-Light Irradiation as a New Method for Defect Passivation in Degraded Perovskite Solar Cells to Recover and Enhance the Performance. *Sci. Rep.* **2019**, *9*, 1–11. [CrossRef] [PubMed]
29. Vágner, P.; Kodým, R.; Bouzek, K. Thermodynamic analysis of high temperature steam and carbon dioxide systems in solid oxide cells. *Sustain. Energy Fuels* **2019**, *3*, 2076–2086. [CrossRef]
30. Xu, H.; Ni, M. High-temperature electrolysis and co-electrolysis. In *Power to Fuel*; Spazzafumo, G., Ed.; Academic Press: Cambridge, MA, USA, 2021; pp. 51–73. [CrossRef]
31. O'Brien, J.E.; Hartvigsen, J.L.; Boardman, R.D.; Hartvigsen, J.J.; Larsen, D.; Elangovan, S. A 25 kW high temperature electrolysis facility for flexible hydrogen production and system integration studies. *Int. J. Hydrogen Energy* **2020**, *45*, 15796–15804. [CrossRef]
32. Hosseini, S.E.; Wahid, M.A. Hydrogen production from renewable and sustainable energy resources: Promising green energy carrier for clean development. *Renew. Sustain. Energy Rev.* **2016**, *57*, 850–866. [CrossRef]